Photoluminescence and Raman studies of α-MoO_3 doped with erbium and neodymium

M. R. Joya[1,*], J. E. Alfonso[1] and L. C. Moreno[2]

[1]Departamento de Física and [2]Departamento de Química, Universidad Nacional de Colombia Bogotá, C.P. 111321, street 45 #30-03, Colombia

With the objective of development of optoelectronic devices, nowadays the research in this field is centred around the study of photoluminescence emission of rare earth elements present in the lattice of different oxides. Therefore, in this study we prepared samples of molybdenum trioxide doped with neodymium and erbium at concentrations of 1.0% and 2.0%, using solid state reaction technique from powders of MoO_3, Nd_2O_3 and Er_2O_3. These powders were analysed by X-ray diffraction which determined the presence of phase α-MoO_3. The morphology of the powders was examined using scanning electron microscopy, which showed that the doped samples have regular and well-defined microplates. The absorption UV-spectra revealed that the optical band gap changed slightly (3.2–3.4 eV) with the Er, Nd and Er–Nd concentrations. The photoluminescence shows emission bands at different wavelengths of the visible spectra as a function of the Er, Nd, and Er–Nd doped. The bands were centred at 748 nm and 808 nm transitions of the Nd^{3+} ions respectively. In this region and with excitation wavelength of 350 nm, strong emission lines were not observed for Er. Raman spectroscopy showed typical modes of vibration of α-MoO_3. Major changes have been noted in the case of samples doped with Er at peaks located between 350 cm^{-1} and 580 cm^{-1}.

Keywords: Erbium, molybdenum trioxide, optical band gap, photoluminescence, neodymium.

MOLYBDENUM trioxide (α-MoO_3), as an intrinsic n-type II–VI semiconductor with wide band gap (~3.2 eV), has been extensively used in organic electronics as an efficient anode with interfacial layers owing to its high work function. Moreover, the MoO_3 nanostructures have also been examined as an effective photocatalyst in pollution degradation[1].

MoO_3 has been used in different applications covering electro-optic to gas sensors[2–7]. Another of the exhibited characteristics of MoO_3 has been its electrochromic properties[8]. These include the reversible change in transmittance and/or reflectance, caused by the application of an externally applied DC voltage, and a change in electrical resistance of the oxide in the presence of gas. In recent years studies have been conducted on the structural, optical and electrical properties of thin films of MoO_3 doped with different elements of transitions, such as titanium and nickel, and/or cobalt[3,4,7]. These focus on improving the electrochromic effect through electron transitions between two kinds of metal sites with different valencies (Ti^{4+}, Ti^{3+}, Mo^{6+}, Mo^{5+}).

Moreover, MoO_3 has been doped with rare earths (REs) such as Er, Er–Yb and Nd ions[5,6,8], with the objective of studying the up-conversion emission and discovering possible applications in the fields of colour display, near-infrared detectors, biological diagnosis, laser cooling and temperature sensors[9–14]. More recently, MoO_3 has been used as a hole injection layer (HIL) in organic light-emitting diodes (OLEDs)[15]. There are several studies available on the physical–chemical properties and applications that have MoO_3 doped and undoped; however, only few studies report evidence of the incorporation of RE ions in the lattice of MoO_3 which explains photoluminescence (PL) emission[16], Raman spectroscopy, UV-Vis and scanning electron microscopy (SEM). Vila *et al.*[17] recently reported effective RE (Er and Eu) incorporation in both MoO_3 nanostructures and bulk crystals.

PL spectra are composed of two broad peaks at 520–570 and 640–680 nm assigned to $(^2H_{11/2}, 4S_{3/2}) \rightarrow 4I_{15/2}$ and $^4F_{9/2} \rightarrow 4I_{15/2}$ transitions of Er^{3+} ions respectively[18]. For neodymium ion we have the 808 nm excitation result in strong emission at 795 nm due to the $^4K_{13/2} \rightarrow {}^4I_{13/2}$ transition along with other emissions from the Nd^{3+} ion[19].

Therefore, in this study we present results for the photoluminescence emission of MoO_3 as a function of Er and Nd (1% and 2%) concentrations. We also discuss the Raman, X-ray, SEM, UV–Vis characteristics of this material.

Experimental methods

Samples of molybdenum trioxide doped with erbium and neodymium were made in atomic concentrations of 1% and 2.0% by the solid-state reaction method from Er_2O_3 (Aldrich 99.99%), Nd_2O_3 (Aldrich 99.99%) and MoO_3 (Merck 99.9%) powders. The stoichiometric amounts of oxides were mixed in isopropanol and subjected to a continuous magnetic agitation process for 8 h, followed by drying process at 80°C. Finally, each sample was subjected to a calcination process for 20 h at 550°C.

*For correspondence. (e-mail: mrinconj@unal.edu.co)

The crystalline structure of these samples was characterized with the aid of an X-ray difractometer (XRD); Panalytical *X*Pert PRO using a Bragg–Brentano geometry with CuKα radiation ($\lambda = 1.5405$ Å) in the 2θ range (10°–70°) with steps of 0.02). A thermionic emission SEM operating at 5.0 kV (Vega3) was used to verify the morphology of the material. Raman scattering spectra were obtained in backscattering geometry JY-T64000 spectrometer for the samples, using the low-power Verdi 532 nm laser line excitation. The UV-Vis spectra were taken (Cary 5000 spectrometer; Varian) in diffuse reflection mode.

The PL measurements were performed with a monospec 27 monochromator (Thermal Jarrel AS, USA) coupled to a R446 photomultiplier (Hamamatsu photonics, Japan). A Krypton ion laser (coherent INNOVA 90 C, USA; $\lambda = 350$ nm) was used as an excitation source.

Results and discussion

Figure 1 shows the XRD patterns of the Er_2O_3–MoO_3 and Nd_2O_3–MoO_3 systems as a function of erbium, neodymium and erbium–neodymium concentrations. The figure also establishes the fact that all crystallographic planes belong to the orthorhombic crystallographic phase of MoO_3 (JCPDS 05-0508). In all the samples an orthorhombic crystallographic phase is observed with the most intense peak corresponding to the plane (040) at 2θ of 25.7°. In the XRD patterns of molybdenum oxide mixing with the RE, there are no planes which belong to the oxides of RE. These results also establish that Er^{3+} and Nd^{3+} ions are integrated at the crystallographic lattice of MoO_3; and they can be confirmed through Raman and PL studies[20–24].

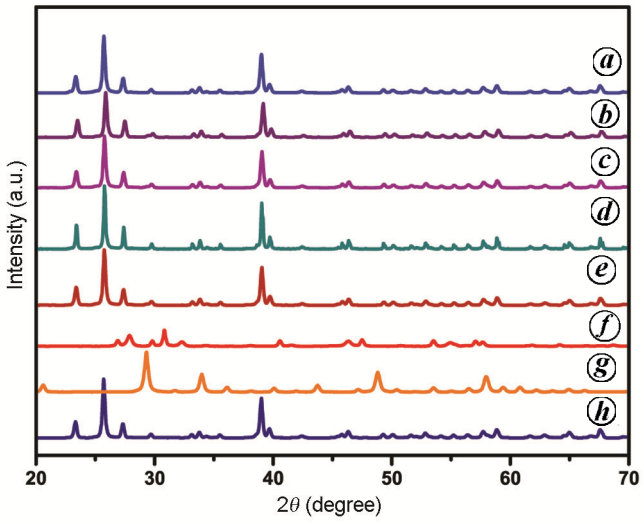

Figure 1. X-ray diffractograms of molybdenum trioxide doped with neodymium and erbium using the solid-state reaction method: ***a***, $Mo_{0.98}Nd_{0.02}O_3$; ***b***, $Mo_{0.98}Er_{0.02}O_3$; ***c***, $Mo_{0.98}Er_{0.01}Nd_{0.01}O_3$; ***d***, $Mo_{0.99}Nd_{0.01}O_3$; ***e***, $Mo_{0.99}Er_{0.01}O_3$, 550°C for 20 h; ***f***, Nd_2O_3; ***g***, Er_2O_3; ***h***, MoO_3, 550°C for 5 h.

Powders processed for 5 and 20 h resulted in the formation of tridimensional microplate structures with different sizes. Figure 2 *a*, *d* and *g* shows the photomicrographs of oxides that were observed, viz. MoO_3, Er_2O_3 and Nd_2O_3 respectively. These samples are agglomerated and shapeless. Nevertheless, Figure 2 *a* shows the presence of several irregular microplates of MoO_3 with agglomerate nature.

Figure 2 *b*, *c*, *e*, *f* and *h* shows photomicrographs of samples doped with Er and Nd. The regular and well-defined microplates indicate that these doped samples have similar morphology. If we compare Figure 2 *c* and *f*, it can be observed that the doping of Er favours the growth of grains with a more defined and regular shape. Figure 2 *d* and *g* shows photomicrographs of erbium and neodymium oxide respectively. These two materials do not have a definite shape in their morphology. They are simple agglomerates of material.

Figure 3 shows the UV-Vis spectra of MoO_3 doped with Er and Nd using the solid-state reaction technique. The optical band gap was determined by extrapolation of the linear portion of the curve or tail. The band gap in the materials is related to absorbance and photon energy. Therefore, the combination of absorbance and photoluminescence measurements helps us to determine energy levels in the materials and the optical band gap. UV–Vis measurements on the six samples give the following values: (a) 3.23 eV (MoO_3), (b) 3.25 eV (Er 1%), (c) 3.27 eV (Nd 1%), (d) 3.25 eV (Er 2%), (e) 3.26 eV (Nd 2%) and (f) 3.32 eV (Er, Nd 1%). The energy gaps are very close; however, with simultaneously increase in erbium and neodymium, the energy gap increases.

The PL property of the samples was measured at room temperature. These materials exhibit a large optical band gap of 3.05 eV, and room temperature photoluminescence at 395 nm (ref. 25). The sample was excited with the laser line at 350 nm (3.54 eV). In Figure 4 *a*, two peaks are observed at 442 nm (2.8 eV, blue) and 475 nm (2.6 eV, bluish-green). The transition at 442 and 475 nm may be attributed to Mo^{5+} (d–d) band transition $d^2_{yz} - d^2_{xz}$ (ref. 26). The emission spectra in Figure 4 *b*, exhibit a series of emission peaks with maxima at ~320–380 nm (UV), ~410–480 nm (blue), ~500–560 nm (green), ~600–660 nm (red) and ~700–800 nm (infrared)[27]. The first major peak at 399 nm corresponds to the radiative relaxation of electrons from the lowest unoccupied molecular orbital to the highest occupied molecular orbital energy levels[27]. Two UV emission bands at 344 and 361 nm were observed by Huan *et al.*[28] corresponding to the transitions of $^4D_{3/2} \rightarrow {}^4I_{9/2}$ and $2P_{3/2} \rightarrow {}^4I_{11/2}$ or $^4D_{3/2} \rightarrow {}^4I_{13/2}$. According to the energy level diagram of Nd^{3+} ion[29], the ion emissions were found at 800 nm ($^4F_{5/2}$, $^2H_{9/2} \rightarrow {}^4I_{9/2}$) and 890 nm ($^4F_{3/2} \rightarrow {}^4I_{9/2}$) (ref. 29).

Figure 4 *c* shows the typical room temperature PL spectrum of Er_2O_3. The transition at 407 nm is due to the electronic transition from $^2H_{9/2} \rightarrow {}^4I_{15/2}$, 450 nm $^4I_{15/2} \rightarrow$

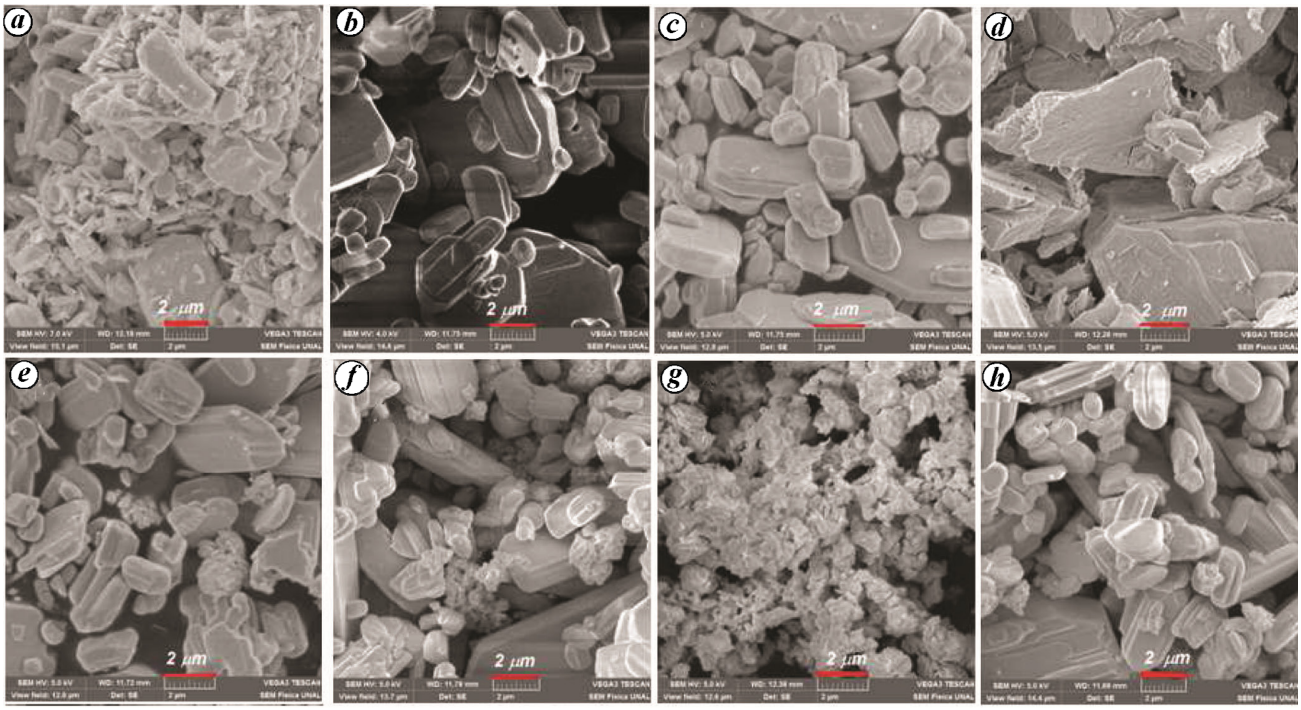

Figure 2. Scanning electron microscope (SEM) photomicrographs of molybdenum trioxide doped with neodymium and erbium using solid-state reaction method: ***a***, MoO_3, 550°C for 5 h; ***b***, $Mo_{0.99}Er_{0.01}O_3$; ***c***, $Mo_{0.98}Er_{0.02}O_3$, 550°C for 20 h; ***d***, Er_2O_3 550°C for 5 h; ***e***, $Mo_{0.99}N\ d_{0.01}O_3$; ***f***, $Mo_{0.98}Nd_{0.02}O_3$, 550°C for 20 h; ***g***, Nd_2O_3, 550°C for 5 h; ***h***, $Mo_{0.98}Er_{0.01}Nd_{0.01}O_3$, 550°C for 20 h.

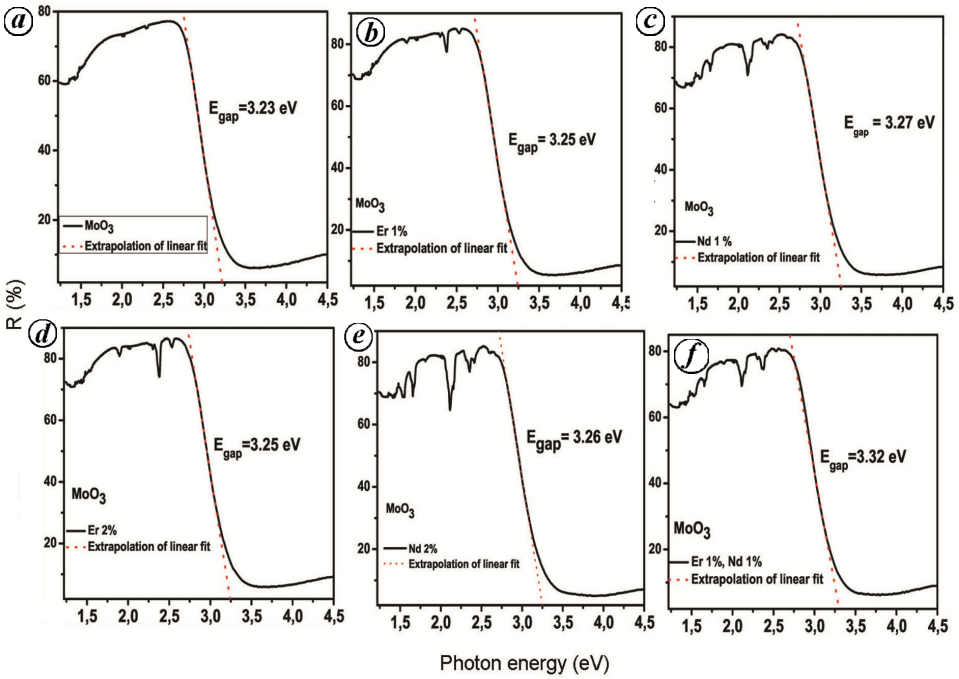

Figure 3. UV–Vis spectra at room temperature: ***a***, MoO_3, 550°C for 5 h; ***b***, $Mo_{0.99}Er_{0.01}O_3$; ***c***, $Mo_{0.99}Nd_{0.01}O_3$; ***d***, $Mo_{0.98}Er_{0.02}O_3$; ***e***, $Mo_{0.98}Nd_{0.02}O_3$; ***f***, $Mo_{0.98}Er_{0.01}Nd_{0.01}O_3$, 550°C for 20 h.

$^4F_{3/2,5/2}$, 487 nm $^4I_{15/2} \rightarrow {}^4F_{7/2}$, 524 nm $^2H_{11/2} \rightarrow {}^4I_{15/2}$ and 540 nm $^2S_{3/2} \rightarrow 4I_{15/2}$. In Figure 4 *c*, an emission at 560 nm also appears as in the literature[30]. It is expected to be the result of relaxation and emission from a higher energy level at an excited state of $^4S_{3/2} \rightarrow {}^4I_{15/2}$. The peak which appears at 680 nm is possibly related to the relaxation processes from $^4F_{9/2} \rightarrow {}^4I_{15/2}$.

Figure 4 *d* and *e* shows the PL spectra of the Er-doped MoO_3 powders. Figure 4 *g* and *h* shows the PL spectra of the Nd-doped MoO_3 powders. As a result of the higher

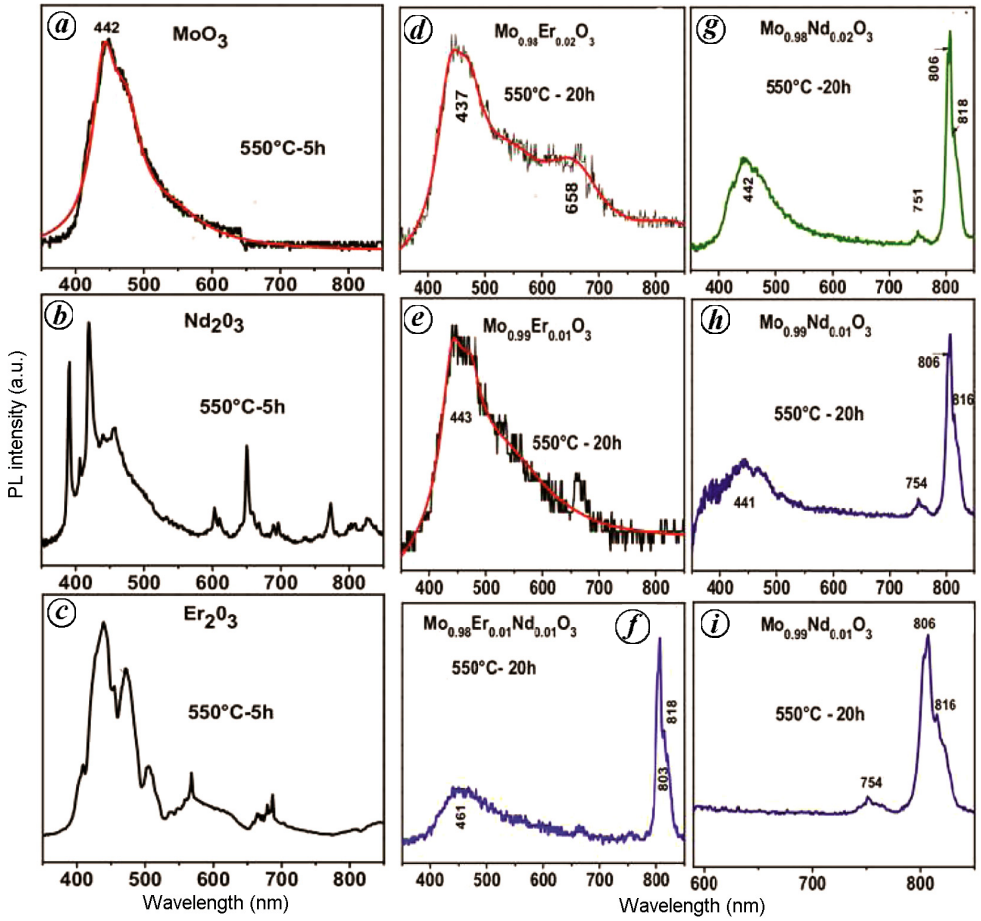

Figure 4. Photoluminescence spectra at room temperature: ***a***, MoO_3; ***b***, Nd_2O_3; ***c***, Er_2O_3, 550°C for 5 h; ***d***, $Mo_{0.98}Er_{0.02}O_3$; ***e***, $Mo_{0.99}Er_{0.01}O_3$; ***f***, $Mo_{0.98}Er_{0.01}Nd_{0.01}O_3$; ***g***, $Mo_{0.98}Nd_{0.02}O_3$; ***h***, $Mo_{0.99}Nd_{0.01}O_3$, 550°C for 20 h; ***i***, magnification of a region in (h).

excitation energy used (350 nm) in Figure 4 *d* and *e*, no emissions were observed in the range 350–800 nm, compared to other studies[31] in which the erbium-doped molybdenum trioxide was excited by a wavelength of 378 nm at room temperature and heat-treated at 600°C. Nevertheless, due to erbium doping (less 2%) the PL peaks were not observed and the material was also heat treated at 500°C for 20 h in an air flow, a treatment similar to that of neodymium. This can be confirmed using Raman spectroscopy. Possibly, for the sample with 2% Er, the 658 nm broadband is related to defects and marks the PL of Er.

In Figure 4 *g* four peaks appear at 442, 751, 806 and 818 nm with 2% Nd. The peak at 806 nm corresponds to the transition of the Nd^{3+} ion ($^4F_{5/2}$, $^2H_{9/2}$ $^4I_{9/2}$) (ref. 32). According to the literature[33,34], absorption peaks are centred at 748 and 808 nm, which are related to the f–d transitions of Nd^{3+} internal ions in the crystal. The absorption bands are attributed to the (748 nm) $^4I_{9/2} \rightarrow {}^4F_{7/2} + {}^4S_{3/2}$ and (808 nm) $^4G_{9/2} \rightarrow {}^4F_{5/2} + {}^4H_{9/2}$ transition of Nd^{3+}. In the present study, it corresponds to the 751 and 806 nm peaks. The difference in peak position may be related to defects in the material. This is indicated by the presence of neodymium in MoO_3. A similar occurrence can be seen with 1% Nd in Figure 4 *h*. Unlike erbium, changes in the photoluminescence with neodymium are more visible. For 1% of erbium and neodymium, graphs in Figure 4 *f* and *h* (1% Nd) are similar, the only difference is that the peak at 754 nm disappears in Figure 4 *f*. These small differences with the other spectra indicate that the dopant material enters the matrix (MoO_3). It is possible to observe the PL for Er^{3+} for wavelengths of a high excitation (808 nm)[34]. However, in the present study, we have used wavelengths under 350 nm.

The irreducible representation of MoO_3 with space group D_{2h} (Pb nm) is given as

$$\Gamma = 8A_g + 8B_{1g} + 4B_{2g} + 4B_{3g} + 4A_u + 3B_{1u} + 7B_{2u} + 7B_{3g}, \quad (1)$$

where A_g, B_{1g}, B_{2g} and B_{3g} are Raman-active modes[35,36]. The Raman-active phonon modes can be used to estimate the structural order at a short range in the materials. Figure 5 *b* shows a typical Raman spectrum of the α-MoO_3 nanoplates. It corresponds to the atomic dispersion of an octahedron (MoO_6) in the phase α-MoO_3. The positions

of these modes can be observed in: 118 (B_{2g}), 129 (B_{3g}), 160 (A_g, B_{1g}), 199 (B_{2g}), 218 (A_g), 247 (B_{3g}), 285 (B_{2g}, B_{3g}), 338 (B_{1g}, A_g), 367 (A_g), 382 (B_{1g}), 472 (A_g, B_{1g}), 667 (B_{2g}, B_{3g}), 820 (A_{g1}, B_{1g}) and 995 (A_{g1}, B_{1g}) cm^{-1}.

The narrow band at 995 cm^{-1} can be assigned to the antisymmetric $\nu(Mo = O_1)$ stretching[35]. The strong band at 820 cm^{-1} represents the symmetric $\nu(Mo–O_3–Mo)$ stretching. The weak and broad bands at 667 and 472 cm^{-1} can be assigned to the antisymmetric $\nu(Mo–O_2–Mo)$ stretching (B_{2g}) and bending (A_g). The bands at 382 and 367 cm^{-1} correspond to the $\delta(O_2 = Mo = O_2)$ scissor. The band at 338 cm^{-1} is a characteristic of the $\delta(O_3–Mo–O_3)$ deformation. The band at 285 cm^{-1} and a weak shoulder centred at 293 cm^{-1} correspond to $\delta(O_1 = Mo = O_1)$ wagging. The bands at 247 and 218 cm^{-1} correspond to the $\delta(O_2–Mo–O_2)$ scissor[35].

Neodymium oxide (Nd_2O_3) material has four phonons ($2A_2u + 2Eu$)[36]. Under room temperature, three Raman bands were observed at 295, 364 and 481 cm^{-1} respectively (Figure 5 *a*). Two wide shoulders were also observed in the 637 and 1076 cm^{-1} positions. The band at 481 cm^{-1} was assigned to the A_2u mode[30].

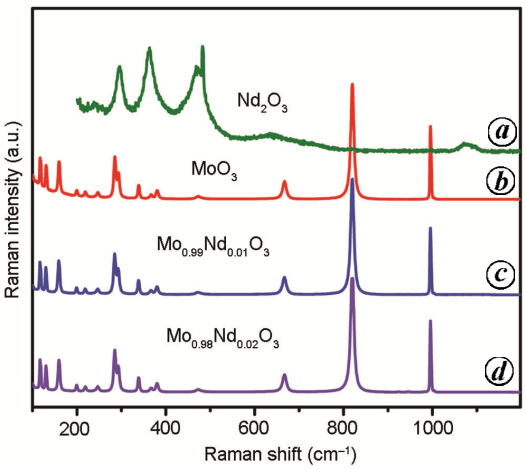

Figure 5. Raman spectra in the range from 100 to 1198 cm^{-1} at room temperature: ***a***, Nd_2O_3; ***b***, MoO_3, 550°C for 5 h; ***c***, $Mo_{0.99}Nd_{0.01}O_3$; ***d***, $Mo_{0.98}Nd_{0.02}O_3$, 550°C for 20 h.

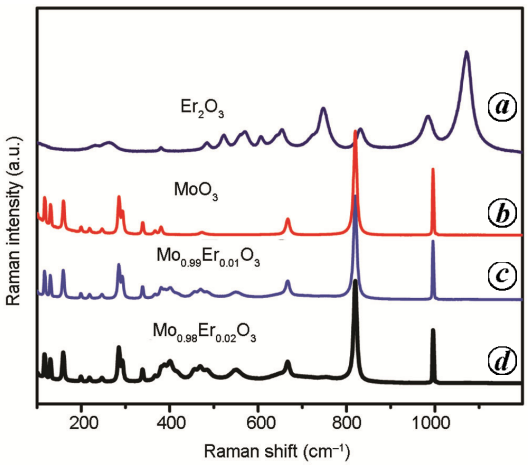

Figure 6. Raman spectra in the range from 100 to 1198 cm^{-1} at room temperature: ***a***, Er_2O_3; ***b***, MoO_3, 550°C for 5 h; ***c***, $Mo_{0.99}Er_{0.01}O_3$; ***d***, $Mo_{0.98}Er_{0.02}O_3$, 550°C for 20 h.

Figure 5 *c* and *d* corresponds to the addition of Nd 1% and 2% respectively. In the Raman spectra for concentrations of 1% an 2% (Nd^{3+}), major changes are not observed. It is difficult to identify vibrational modes in the fluorescent emissions that overlap the Raman spectrum in the lattice area with the 514 nm (ref. 30). In order to excite the samples in the present study, a green laser (532 nm) was used. This may be a possible justification of why not many changes are observed in the Raman spectrum of MoO_3 with neodymium doping.

Figure 6 *a* shows spectra obtained from Er_2O_3 using a 532 nm excitation. The bands at 232, 262, 381, 484, 522, 565, 606, 653, 725, 746, 831, 983 and 1071 cm^{-1} correspond to the Raman bands for Er_2O_3. Figure 6 *b* corresponds to MoO_3, and the Raman modes have already been explained in Figure 5 *b*. Figure 6 *c* and *d* corresponds to the spectra of molybdenum trioxide doped with erbium 1% and 2% respectively. The Er^{3+} ions in the material MoO_3 induce partial structural amorphization of the samples as evidenced by the spectra in the region between 370 and 580 cm^{-1}. The three peaks that appear in the Raman spectra for the two erbium concentrations are wide. This is an indication that Er ions are incorporated into the material. In the case of PL (Figure 4), this effect had not been observed. However, in Figure 6 *c* and *d* these new peaks indicate the effects of erbium doping. These new peaks appear at positions 401, 416, 456, 485 and 550 cm^{-1}.

Conclusion

In the present work, the incorporation of Er and Nd to MoO_3 was studied, by means of the comparison of the Raman spectra and the PL emission, of the doped and undoped samples. These measurements made with excitation line of 350 nm, show a band centred at 443 nm for MoO_3 doped with Er, at 806 nm for samples doped with Nd, and at 803 nm for samples doped with Er–Nd: these are different from emission band of the oxides, centred at 442 nm (MoO_3), and emission band between 400 and 600 nm in neodymium and erbium oxide. These results suggest that MoO_3 doped with the Er and Nd can be used to develop middle infrared optical devices. Moreover, Raman spectra excited at 532 nm, showed major changes in low-frequency modes with increased doping of Er. Three new peaks at 400, 480 and 550 cm^{-1} were observed. These results suggest that the erbium ions be incorporated into the MoO_3 causing defects in their lattice. XRD shows the orthorhombic phase in the doped samples. SEM measurements showed that the doping of Er and Nd favours the growth of grains, with a more defined and regular shape compared to the MoO_3 sample. However, the energy band gap of the samples increases with the concentration of Er and Nd compared to the pure sample of MoO_3.

1. Xiang, D., Han, C., Zhang, J. and Chen, W., Gap states assisted MoO_3 nanobelt photodetector with wide spectrum response. *Sci. Rep*., 2014, **4**, 4891.
2. Ma, K., Yin, J., Zhang, Q. and Xie, J., Thermal stability and photoluminescence property of hexagonal $MoO_3 : 0 : 55H_2O_2$ microrods. *Phase Transitions*, 2016, **90**, 342.
3. Mahajan, S. S., Mujawar, S. H., Shinde, P. S., Inamdarb, A. I. and Patilb, P. S., Structural, morphological, optical and electrochromic properties of Ti-doped MoO_3 thin films. *Sol. Energ. Mater. Sol. Cells*, 2009, **93**, 183.
4. Pereira, L. G. *et al.*, Influence of doping on the preferential growth of α-MoO_3. *J. Alloys Compd.*, 2008, **459**, 377.
5. Ren, P. *et al.*, Green photoluminescence from erbium-doped molybdenum trioxide. *Mater. Lett*., 2014, **122**, 320.
6. Dong, B., Li, Z., Cao, B., Yu, N. and Sun, M., Quasi-one dimensional $Er^{3+}Yb^{3+}$ codoped single-crystal MoO_3 ribbons: synthesis, characterization and up-conversion luminescence. *Opt. Commun*., 2011, **284**, 2528.
7. Li, Z., Wang, W., Zhao, Z., Liu, X. and Song, P., One-step hydrothermal preparation of Ce-doped MoO_3 nanobelts with enhanced gas sensing properties. *RSC Adv*., 2017, **7**, 28366.
8. Alfonso, J. E., Garzon, R. and Moreno, L. C., Behaviour of the thermal expansion coefficient of α-MoO_3 as a function of the concentration of the Nd^{3+} ion. *Physica B: Condens. Mater.*, 2012, **407**, 4001.
9. Wang, F. *et al.*, Simultaneous phase and size control of upconversion nanocrystals through lanthanide doping. *Nature*, 2010, **463**, 1061.
10. Sun, C. J., Xu, Z. H., Hu, B., Yi, G. S., Chow, G. M. and Shen, J., Application of $NaYF_4 : Yb$, Er upconversion fluorescence nanocrystals for solution-processed near infrared photodetectors. *Appl. Phys. Lett*., 2007, **91**, 191113.
11. Chatterjee, D. K., Rufaihah, A. J. and Zhang, Y., Upconversion fluorescence imaging of cells and small animals using lanthanide doped nanocrystals. *Biomaterials*, 2008, **29**, 937.
12. Wang, G. F., Peng, Q. and Li, Y. D., Upconversion luminescence of monodisperse $CaF_2 : Yb^{3+}/Er^{3+}$ nanocrystals. *J. Am. Chem. Soc*., 2009, **131**, 14200.
13. Garcia-Adeva, A. J., Balda, R. and Fernandez, J., Upconversion cooling of Er-doped low-phonon fluorescent solids. *Phys. Rev. B*, 2009, **79**, 033110.
14. Dong, B., Liu, D. P., Wang, X. J., Yang, T., Miao, S. M. and Li, C. R., Optical thermometry through infrared excited green upconversion emissions in $Er^{3+}Yb^{3+}$ codoped Al_2O_3. *Appl. Phys. Lett*., 2007, **90**, 181117.
15. Yun, J., Yang, J., Hong, Y. and Lee, C., Low driving voltage and long lifetime organic light-emitting diodes with molybdenum oxide (MoO_3) doped hole transport layer. *J. Korean Phys. Soc*., 2008, **53**, 1660.
16. Rao, L. S., Rao, P. V., Sharma, M. V. N. V. D. and Veeraiah, N., J–O parameters versus photoluminescence characteristics of $40Li_2O4MO$ (MON b_2O_5, MoO_3 and WO_3)-$55B_2O_3 : 1N$ d_2O_3 glass systems. *Optik – Int. J. Light Electron Opt.*, 2017, **142**, 674.
17. Vila, M., Diaz-Guerra, C., Jerez, D., Lorenz, K., Piqueras, J. and Alves, E., Intense luminescence emission from rare-earth-doped MoO_3 nanoplates and lamellar crystals for optoelectronic applications. *J. Phys. D*, 2014, **47**, 355105.
18. Dehdouh, H., Bensaha, R. and Zergoug, M., Structural modification, photoluminescence, and magnetic property enhancement with Er^{3+} doping, of sol–gel TiO_2 thin films. *Mater. Res. Express*, 2017, **4**, 086408.
19. Sukul, P. P. and Kumar, K., Near infrared (808 and 980 nm) excited photoluminescence study in Nd-doped Y_2O_3 phosphor for bio-imaging. *Methods Appl. Fluoresc.*, 2016, **4**, 44005.
20. Rudolph, W. W. and Irmerb, G., Raman spectroscopic characterization of light rare earth ions: La^{3+}, Ce^{3+}, Pr^{3+}, Nd^{3+} and Sm^{3+} hydration and ion pair formation. *Dalton Trans*., 2017, **46**, 4235.
21. Rao, M. C., Ravindranadh, K., Kasturi, A. and Shekhawat, M. S., Structural stoichiometry and phase transitions of MoO_3 thin films for solid state microbatteries. *Res. J. Recent Sci*., 2013, **2**, 67.
22. Nagabhushana, G. P., Samrat, D. and Chandrappa, G. T., α-MoO_3 nanoparticles: solution combustion synthesis, photocatalytic and electrochemical properties. *RSC Adv*., 2014, **4**, 56784.
23. Dagar, J., Tyagi, P., Ahmad, R., Singh, R., Sinha, O. P., Sumana, C. K. and Srivastava, R., Application of 2D-MoO_3 nano-flakes in organic light emitting diodes: effect of semiconductor to metal transition with irradiation. *RSC Adv*., 2015, **5**, 8397.
24. Gillaspie, D. T., Tenent, R. C. and Dillon, A. C., Metal-oxide films for electrochromic applications: present technology and future directions. *J. Mater. Chem*., 2010, **20**, 9585.
25. Zhao, Y., Liu, J., Zhou, Y., Zhang, Z., Xu, Y., Naramoto, H. and Yamamoto, S., Preparation of MoO_3 nanostructures and their optical properties. *J. Phys.: Condens. Matter*, 2003, **15**, L547.
26. Navas, I., Vonodkumar, R. and Pillai, V. P. M., Self-assembly and photoluminescence of molybdenum oxide nanoparticles. *Appl. Phys. A*, 2011, **103**, 373.
27. Goel, P. and Arora, P., Mechanism of photoluminescence enhancement and quenching in Nd_2O_3 nanoparticles ferroelectric liquid crystal nanocomposites. *RSC Adv*., 2015, **5**, 14974.
28. Huan, R. J., Gang, Z. T., Huan, L. J., Juan, K., Xin, H. J. and Lin, G., Synthesis and photoluminescence properties of Nd_2O_3 nanoparticles modified by sodium *bis*(2-ethylhexyl) sulfosuccinate. *Chin. Phys. B*, 2008, **17**, 4669.
29. Ha, D. H., Kim, H. J., Park, J. M. and Kaewao, J., Luminescence properties of Nd_2O_3-doped gadolinium-borate glass scintillators. *New. Phys. Sae Mulli*, 2015, **65**, 255.
30. Cui, J. and Hopex, G. A., Raman and fluorescence spectroscopy of CeO_2, Er_2O_3, Nd_2O_3, Tm_2O_3, Yb_2O_3, La_2O_3 and Tb_4O_7. *J. Spectrosc*., 2015, **2015**, 1.
31. Zhang, K., Teng, F., Zhang, Z. and Yan, P. X., Green photoluminescence from erbium-doped molybdenum trioxide. *Mater. Lett*., 2014, **122**, 320.
32. Tian, G., Gu, Z., Zhao, Y. and Ma, Y., Elimination of photon quenching by a transition layer to fabricate a quenching-shield sandwich structure for 800 nm excited upconversion luminescence of Nd^{3+}-sensitized nanoparticles. *Adv. Mater.*, 2014, **26**, 2831.
33. Zhang, M., Guo, H., Han, J., Zhang, H. and Xu, C., Distribution of neodymium and properties of Nd : YAG crystal by horizontal directional solidification. *J. Crystal. Growth*, 2012, **340**, 130.
34. Tian, L., Xu, Z., Zhao, S., Cui, Y., Liang, Z., Zhang, J. and Xu, X., The upconversion luminescence of $Er^{3+}/Yb^{3+}/Nd^{3+}$ triply-doped $NaYF_4$ nanocrystals under 808 nm excitation. *Materials*, 2014, **7**, 7289.
35. Chen, D. *et al.*, Single-crystalline MoO_3 nanoplates: topochemical synthesis and enhanced ethanol-sensing performance. *J. Mater. Chem.*, 2011, **21**, 9332.
36. Windom, B. C., Sawyer, W. G. and Hahn, D. W., A Raman spectroscopic study of MoS_2 and MoO_3: applications to tribological systems. *Tribal. Lett*., 2011, **423**, 301.

ACKNOWLEDGEMENTS. We thank the National University of Colombia, Bogotá. We also thank Profs Paulo De Tarso (UFC-Brazil) and Máximo Li (USP-Brazil) for fruitful discussions and measurements.

Received 15 November 2017; revised accepted 15 February 2019

doi: 10.18520/cs/v116/i10/1690-1695